Bioorganic Chemistry 82 (2019) 274–283

Contents lists available at ScienceDirect

Bioorganic Chemistry

journal homepage: www.elsevier.com/locate/bioorg

Bioactive scalemic caged xanthones from the leaves of *Garcinia bracteata*

Bao-Jun Zhang[a,b,c,1], Wen-Wei Fu[a,b,1], Rong Wu[a,b], Jin-Ling Yang[a,b], Cai-Yun Yao[d], Bing-Xiong Yan[d], Hong-Sheng Tan[a,b], Chang-Wu Zheng[a,b], Zhi-Jun Song[d,*], Hong-Xi Xu[a,b,*]

[a] School of Pharmacy, Shanghai University of Traditional Chinese Medicine, Shanghai 201203, People's Republic of China
[b] Engineering Research Center of Shanghai Colleges for TCM New Drug Discovery, Shanghai 201203, People's Republic of China
[c] Departement of Pharmacy, Shanghai Putuo District People Hospital, Shanghai 200060, People's Republic of China
[d] Guangxi Botanical Garden of Medicinal Plants, Nanning 530023, People's Republic of China

ARTICLE INFO

Keywords:
Garcinia bracteate
Caged xanthones
Garcibractatin A
Cytotoxicity

ABSTRACT

Four pairs of previously undescribed caged xanthones (**1–4**) and twelve known caged xanthones (**5–16**) were isolated from the leaf extract of *Garcinia bracteata*. Their structures were unambiguously elucidated on the basis of spectroscopic methods. The planar structure and relative configuration of **1** was confirmed by X-ray crystallographic analysis. The enantiomers of compounds **1**, **2**, **4** were further resolved by semi-preparative chiral HPLC, and the absolute configurations of enantiomers of compounds **1** and **4** were determined by measurement and calculation of electronic circular dichroism (ECD) spectra and specific rotations. The inhibitory activities of the isolated compounds against human HeLa, A549, PC-3, HT-29, and WPMY-1 cell lines were assayed, and garcibractatin A (**4**) showed the most potent inhibitory activities *in vitro* with IC_{50} values from 1.11 to 2.93 μM. A preliminary structure-activity relationship has been discussed, and some helpful conclusions have been drawn.

1. Introduction

Natural products (NPs) have played a key role in drug discovery, as they are often represented as the source of drugs or drug leads [1–4]. Approximately 33% of the therapeutic agents launched were developed or derived from NPs in the period of 1981–2014 [4]. In the case of anticancer drugs, approximately 60% of the therapeutic agents currently used in the cancer chemotherapy have natural origin [5,6]. Thus, NPs could serve as a prolific source or as a "source of inspiration" for the discovery of anticancer drugs and identification of new anticancer NPs would be helpful for improving cancer chemotherapy.

During our continuous effort to identify anticancer agents present in natural sources [7–14], we found that, among extracts obtained from various parts of 14 native Chinese *Garcinia* plants, the 95% EtOH extract of the leaves of *Garcinia bracteata* C. Y. Wu ex Y. H. Li. (Clusiaceae) exhibited strong cytotoxic activity against ten human cancer cell lines, and the two caged xanthones from the trunks of *G. bracteata* can significantly induce apoptosis and inhibit autophagy [14]. *G. bracteata*, a tree approx. 8 mtall, is distributed mainly in the southern regions of Yunnan and Guangxi Provinces of China [15]. Plants of *G. bracteata* generate various classes of secondary metabolites such as prenylated xanthones [16–19,21,22], benzophenones [17], isoprenylated flavones and biphenyl derivatives [20]. Caged xanthones, a special group of polyprenylated xanthones with an unusual 4-oxatricyclo [4.3.1.03,7] dec-2-one skeleton, have been isolated as the major secondary metabolites from the plant and showed strong cytotoxic activities [14,16–18,22]. Due to intriguing structures and strong cytotoxic activities, the caged xanthones have attracted increasing attentions. Several scalemic caged xanthones had been identified recently from the plant [22] and two corresponding enantiomers of scalemic caged xanthones might show the different cytotoxic cytotoxicity [23]. These findings prompted us to initiate our further investigation of caged xanthones present in *G. bracteata*.

Following our previous success in identifying active ingredients with cytotoxicity from the native Chinese *Garcinia* plants, we herein report four pairs of previously undescribed caged xanthones (**1–4**), and 12 known caged xanthones (**5–16**) (Fig. 1), isolated from an extract of the leaves of *G. bracteata*. The inhibitory activities of these isolates against HeLa, A549, PC-3, HT-29 and WPMY-1 cells were assayed, and the preliminary structure-activity relationship had been discussed. In this report, the isolation of these compounds, the elucidation of their

* Corresponding authors at: School of Pharmacy, Shanghai University of Traditional Chinese Medicine, Cai Lun Lu 1200, Shanghai 201203, People's Republic of China (H.-X. Xu). Guangxi Botanical Garden of Medicinal Plants, Chang Gang Lu 189, Nanning 530023, People's Republic of China (Z.-J. Song).
E-mail addresses: 88519368@qq.com (Z.-J. Song), xuhongxi88@gmail.com (H.-X. Xu).
[1] These authors contributed equally to the work and should be regarded as equivalent first authors.

https://doi.org/10.1016/j.bioorg.2018.10.041
Received 6 July 2018; Received in revised form 18 October 2018; Accepted 22 October 2018
Available online 25 October 2018
0045-2068/

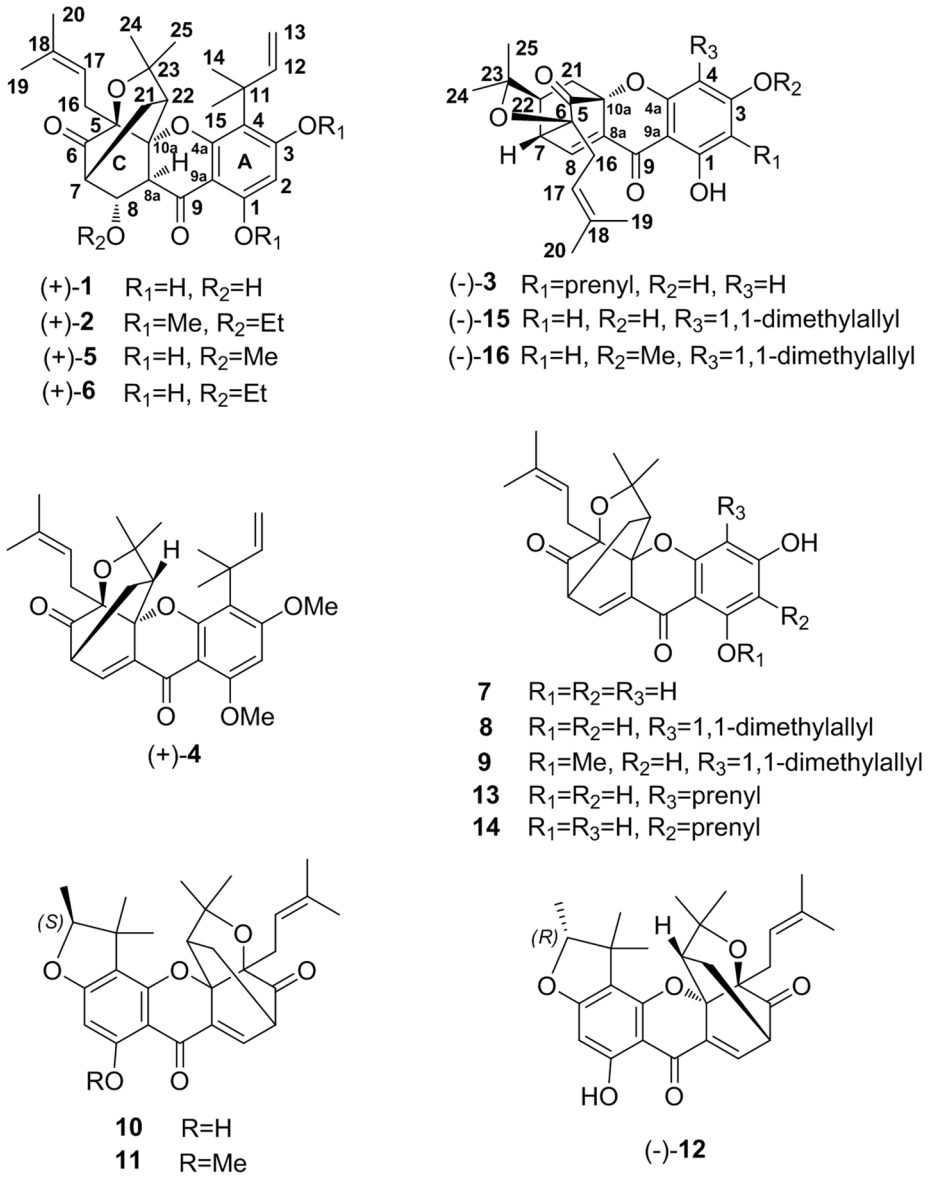

Fig. 1. Chemical structures of compounds **1–16**.

structures and their inhibitory effects on the proliferation of human cancer cells are described.

2. Experimental section

2.1. General experimental procedures

Optical rotations were measured using an AUTOPOL VI 90079 Automatic Polarimeter (Rudolph Research Analytical, Hackettstown, NJ). IR spectra were obtained on a Nicolet 6700 spectrophotometer. ECD spectra were measured on a Chirascan v.4.2.17 spectropolarimeter (Applied Photophysics, U.K.) or Jasco J-810CD Spectropolarimeter (JASCO Corp., Tokyo, Japan). HPLC-ECD analysis was carried out on an HPLC system (LC-2000, Jasco), consisting of a diode-array detector (MD-2010, Jasco), quaternary gradient pump (PU-2089, Jasco), and auto-sampler (AS-2055, Jasco), connected to an ECD detector (CD-2095, Jasco). HR-ESI-Q-TOF-MS experiments were performed on a SYNAPT G2-Si HDMS (Waters Corp., Manchester, UK) equipped with an electrospray ionization source. The crystallographic data were obtained on a Bruker SMART APEX-II CCD diffractometer equipped with graphite monochromatized Cu Kα radiation (λ = 1.54178 Å for **1**) or Mo Kα radiation (λ = 0.71073 Å for **5**). NMR spectra were recorded on a Bruker Avance-600 spectrometer and calibrated based on the solvent peak used. Analytical HPLC was performed on a Waters 2535 Series machine equipped with an Xbridge C18 column (4.6 × 250 mm, 5 μm), and preparative HPLC was performed on a preparative Xbridge Prep C18 OBD column (19 × 250 mm, 5 μm). Column chromatography was performed on CHP20P MCI gel (75–150 μm, Mitsubishi Chemical Corporation, Japan), silica gel (200–300 mesh, Qingdao Haiyang Chemical Co., Ltd.), Sephadex LH-20 (GE Healthcare Bio-Sciences AB, Sweden), and reversed-phase C18 silica gel (50 μm, YMC, Kyoto, Japan). Analytical and preparative TLC was performed on pre-coated GF254 plates (0.25- or 0.5-mm thickness, Qingdao Haiyang Chemical Co. Ltd.). Detection was performed by spraying the plates with 10% sulfuric acid followed by heating.

2.2. Plant material

Leaves of *Garcinia bracteata* were collected from Napo, Guangxi Province, People's Republic of China, in October 2012, and authenticated by Professor Zhao Yiming, Guangxi Medicinal Garden. A voucher specimen (ERCSC-2012 GB1001) was deposited at the Engineering Research Center of Shanghai Colleges for TCM New Drug Discovery.

2.3. Extraction and isolation

Air-dried and powdered leaves of the plant (7.2 kg) were extracted with 95% EtOH (v/v, 5 × 12 L, two days each time) at room temperature. The combined EtOH extracts were concentrated *in vacuo* to yield a brown-yellow gum (2.6 kg). The 95% ethanol-soluble portion was suspended in H_2O (10 L) and extracted with petroleum ether (3 × 10 L) to yield a petroleum ether-soluble portion (700 g) and a H_2O-soluble portion. The petroleum ether-soluble portion was chromatographed on an MCI gel column, eluting with EtOH-H_2O (v/v, 20:80, 85:15, and 95:5, successively) to yield the 85% ethanol-soluble portion (65 g). The 85% ethanol-soluble portion was subjected to silica gel column chromatography (CC) in a gradient of petroleum ether-EtOAc (1:0–1:4, v/v); this procedure yielded 19 fractions (F1-F19) based on the TLC profiles.

F9 (Fraction 9) was first separated by Sephadex LH-20 in $CHCl_3$-MeOH (1:1), yielding ten sub-fractions (F9.1 − F9.10); White precipitates (ca. 32 mg) from the sub-fraction F9.3 were further purified by preparative HPLC (MeCN-H_2O, 60:40, 15 mL/min), yielding compounds **5** (10.56 mg) and **6** (10.87 mg); F11 was subjected to Sephadex LH-20 column and eluted with a $CHCl_3$-MeOH (1:1) mixture of solvents to give 18 sub-fractions (F11.1 − F11.18). Sub-fraction F11.7 (35 mg) was further purified by preparative HPLC (35 min, 60% MeCN in H_2O → 95% MeCN in H_2O, 10 mL/min), yielding compound **1** (12.36 mg); F14 was chromatographed separately on a Sephadex LH-20 column and eluted with $CHCl_3$-MeOH (1:1) to afford ten sub-fractions (F14.1-F14.10) based on TLC profiles. Compound **2** (8.65 mg) was deposited from the sub-fraction F14.6 (ca. 151 mg) in ethyl acetate solution, and F14.8 (41 mg) was further purified by preparative HPLC (MeCN-H_2O, 50:50, 15 mL/min), yielding compound **11** (6.52 mg).

Air-dried and powdered leaves of the plant (341.7 g) were refluxed with 95% EtOH (v/v, 5 × 2.4 L). The combined EtOH extracts were concentrated *in vacuo* to yield a brown-yellow gum (116.45 g). The 95% ethanol-soluble fraction was dissolved in the lower phase of *n*-hexane-ethyl acetate-95% ethanol-water (1:1:1:1, v/v/v/v), which was extracted three times with equal volume of the upper phase, and the upper phase was combined and concentrated *in vacuo* to obtain as the upper phase-soluble fraction (19.13 g). At the same time, the yellow precipitates from the two-phase boundary were collected as the insoluble fraction (13 g).

The yellow insoluble fraction was subjected to silica gel CC in a gradient of petroleum ether-EtOAc (1:0–0:1, v/v) to yield 12 fractions (IF1-IF12) based on the TLC profiles. IF6 (the insoluble fraction 6, 83 mg) was further purified by preparative HPLC (40 min, 40% MeCN in H_2O → 100% MeCN, 15 mL/min), yielding compounds **3** (2.56 mg) and **14** (10.6 mg); IF7 (56 mg) was further purified by preparative HPLC (40 min, 40% MeCN in H_2O → 100% MeCN, 15 mL/min), yielding compounds **7** (6.75 mg) and **14** (4.86 mg); IF8 (103 mg) was further purified by preparative HPLC (40 min, 40% MeCN in H_2O → 100% MeCN, 15 mL/min), yielding compound **13** (5.53 mg).

The upper phase-soluble fraction was separated on Sephadex LH-20 in $CHCl_3$ − MeOH (1:1), yielding 16 sub-fractions (UF1 − UF16). UF3 (the upper phase-soluble fraction 3, 72 mg) was purified by preparative HPLC (40 min, 40% MeCN in H_2O → 100% MeCN, 15 mL/min), yielding compound **4** (10.23 mg); UF4 (26 mg) was purified by preparative HPLC (40 min, 40% MeCN in H_2O → 100% MeCN, 15 mL/min), yielding compound **9** (8.71 mg); UF5 (963 mg) was first separated by preparative HSCCC (*n*-hexane-ethyl acetate-95% ethanol-water, 1:1:1:1, v/v/v/v; 852 rpm, 2 mL/min), yielding sub-fractions UF5.1 (105.54 mg) and UF5.2 (20.88 mg). Sub-fraction UF5.1 was further purified by preparative HPLC (MeCN-H_2O, 60:40, 15 mL/min), yielding compounds **10** (89.61 mg) and **12** (8.35 mg). UF5.2 was further purified by preparative HPLC (40 min, 40% MeCN in H_2O → 100% MeCN, 15 mL/min), yielding compound **16** (10.31 mg). UF6 (138 mg) was further separated by preparative HSCCC (*n*-hexane-ethyl acetate-95% ethanol-water, 6:4:7:3, v/v/v/v; 850 rpm, 2 mL/min), yielding compound **15** (56.04 mg).

2.4. Chiral HPLC-ECD analysis of compounds *1–4* and chiral HPLC separation of compounds *1, 2, 4–6*

HPLC-ECD analysis was carried out on an online HPLC-DAD-CD system. The resolution of the compounds **1–4** at the analytical scale was achieved on an AD-H (Daicel Chiralpak AD-H, 5 μm, 4.6 × 250 mm) or OD-H (CHIRACEL OD-H, 5 μm, 4.6 × 250 mm) chiral column. Detection was carried out with a wavelength set to 254 nm. The mobile phase was *n*-hexane:2-propanol in the ratio 90:10 for **1**, **3** and **4**, and 95:5 for **2** with a flow rate of 1.0 mL/min. Compounds **1**, **3**, and **4** were analyzed on AD-H chiral column to yield two well-solved peaks for the enantiomers at retention times of t_R 11.9 and 17.3 min in an approximate ratio of 1:1.8 for **1**, at retention times of t_R 7.4 and 15.6 min in an approximate ratio of 1:1.1 for **3**, and at retention times of t_R 9.9 and 11.1 min in an approximate ratio of 1:1 for **4**. Compound **2** was subjected to chiral HPLC on OD-H chiral column give two well-solved peaks for the enantiomers at retention times of t_R 14.0 and 15.3 min in an approximate ratio of 1.1:1 for **2**. The ECD spectra of the eluent at the retention time of each peak were subtracted from the ECD curves of the compounds analyzed.

Scalemic mixtures of compounds **1** (5.8 mg), **2** (2.1 mg), and **4** (8.6 mg) were subjected to HPLC using the conditions described for HPLC-ECD analysis to yield pure enantiomers. Owing to an insufficient amount of material, the pure enantiomers of compound **3** could not be resolved. The enantiomers of compounds **5** and **6** were resolved by chiral HPLC to obtain the pure enantiomers for cell proliferation assays on human cancer cells. Resolution of the two enantiomers of **5** (5.3 mg) and **6** (4.2 mg) were performed by the method described for **1**, to give compounds (−)-**5** [t_R 7.44 min, 1.6 mg, $[\alpha]_D^{25}$ –62 (*c* 0.12, MeCN)]; (+)-**5** [t_R 15.58 min, 2.9 mg, $[\alpha]_D^{25}$ + 19 (*c* 0.15, MeCN)]; (−)-**6** [t_R 9.86 min, 0.67 mg, $[\alpha]_D^{25}$ –4.8 (*c* 0.09, MeCN)]; and (+)-**6** [t_R 11.13 min, 2.55 mg, $[\alpha]_D^{25}$ + 34 (*c* 0.177, MeCN)].

2.4.1. Garcibractone A (*1*)

White amorphous powder; $[\alpha]_D^{20}$ -20.834 (*c* 0.12, MeCN); UV (MeOH) λ_{max} (log ε) 204 (4.23), 210 (4.19), 217 (4.22), 256 (3.20), 297 (4.06) and 396 (2.80) nm; IR (KBr) ν_{max} 3535, 3406, 2970, 2970, 1737, 1639, 1618, 1591, 1496, 1462, 1414, 1388, 1271, 1184, 1022, 823, 577 cm^{-1}; ^1H NMR (DMSO-d_6, 600 MHz) and ^{13}C NMR (DMSO-d_6,150 MHz) data, see Tables 1 and 2; HRESIMS *m/z* 483.2387 $[M+H]^+$ (calcd for $C_{28}H_{35}O_7$, 483.2383).

(−)-*Garcibractone A* (***1a***): t_R 17.3 min, 2.0 mg, $[\alpha]_D^{26}$ + 9.63 (*c* 0.02, MeOH); ECD (MeOH) λ_{max} nm (Δε): 221 (+2.67 × 10^2), 307 (−2.45 × 10^2) nm.

(+)-*Garcibractone A* (***1b***): t_R 11.9 min, 1.8 mg, $[\alpha]_D^{26}$ − 9.33 (*c* 0.018, MeOH); ECD (MeOH) λ_{max} nm (Δε) 221 (−1.82 × 10^2), 305 (+1.92 × 10^2).

2.4.2. Garcibractone B (*2*)

White amorphous powder; $[\alpha]_D^{20}$ 0.91 (*c* 0.1, MeCN); UV (MeOH) λ_{max} (log ε) 204 (4.35), 219 (4.37), and 291 (4.23) nm; IR ν_{max} 2972, 2931, 2871, 1731, 1675, 1589, 1556, 1468, 1378, 1317, 1272, 1212, 1171, 1148, 1111, 1038, 1006, 966, 898, 856, 816, 803, 674, 568, 451 cm^{-1}; ^1H NMR (DMSO-d_6, 600 MHz) and ^{13}C NMR (DMSO-d_6, 150 MHz) data, see Tables 1 and 2; ESITOFMS *m/z* 539.3010 $[M+H]^+$ (calced for $C_{32}H_{43}O_7$, *m/z* 539.3009).

(−)-*Garcibractone B*(***2a***): t_R = 15.2 min, 0.9 mg, $[\alpha]_D^{25}$ –23.33 (c 0.09, MeCN)]; ECD λ_{max} nm (mdeg): 232 (31.47), 308 (-9.35) nm.

(+)-*Garcibractone B*(***2b***): t_R 13.8 min, 0.84 mg, $[\alpha]_D^{25}$ + 24.44 (*c* 0.09, MeCN)]; ECD λ_{max} nm (mdeg): 230 (-39.04), 308 (+11.31) nm.

Table 1
^{1}H (600 MHz) and ^{13}C (150 MHz) NMR spectral data of **1–4.**[a]

Position	**1**[b]		**2**[b]		**3**[b]		**4**[c]	
	δ_C	δ_H	δ_C	δ_H	δ_C	δ_H	δ_C	δ_H
1	161.7		160.5		161.1		161.1	6.14, s
2	97.3	5.98, s	91.0	6.34, s	108.4		90.7	
3	167.1		165.1		164.6		165.5	
4	113.2		114.5		95.2	6.01, s	115.7	
4a	157.9		158.4		158.9		161.5	
5	86.4		86.0		200.1		84.9	
6	210.1		209.5		78.9		204.8	
7	47.8	2.46, dd (6.0, 4.6)	44.6	2.68, m	44.3	3.78, dd (6.8, 4.4)	49.3	3.39, t (5.8)
8	65.6	4.53, ddd (4.7, 3.2, 1.5)	72.8	4.36, dd (4.3, 1.4)	133.5	7.15, d (6.8)	131.9	7.28, d (6.7)
8a	49.7	3.14, d (1.4)	48.1	3.06, s	134.5		136.4	
9	195.2		186.6		178.9		176.1	
9a	101.8		104.7		99.3		105.7	
10a	88.6		87.7		83.3		91.6	
11	40.9		40.7		20.6	3.09, d (7.3)	41.6	
12	150.0	6.12, dd (17.4, 10.6)	150.4	6.15, dd (17.6, 10.4)	122.7	5.11, dd (7.3, 5.9)	151.0	6.14, dd (17.4, 10.6)
13	108.5	4.80, dd (17.4, 1.3)	107.5	4.76, d (17.6)	129.6		106.8	4.75, d (10.6)
		4.79, dd (10.6, 1.3)		4.74, d (10.4)				4.69, d (17.4)
14	30.3	1.54, s	30.9	1.57, s	25.4	1.60, s	31.1	1.66, s
15	29.0	1.52, s	28.7	1.52, s	17.6	1.68, s	28.0	1.62, s
16	27.6	2.68, dd (15.1, 5.9)	27.4	2.71, m	29.9	2.29, m	28.8	2.65, dd (15.0, 5.4)
		2.53, dd (15.0, 8.3)		2.57, dd (14.9, 8.6)		2.04, dd (14.5, 8.2)		2.56, dd (14.4, 9.3)
17	119.3	5.38, m	118.5	5.29, t (7.1)	117.6	4.92, dd (8.5, 7.0)	117.9	4.49, m
18	132.0		131.8		135.2		134.9	
19	18.1	1.54, s	17.7	1.55, s	17.8	1.55, s	25.7	1.18, s
20	26.1	1.60, s	25.7	1.61, s	25.6	1.65, s	17.4	1.42, s
21	20.4	1.78, dd (14.6, 6.1)	19.4	2.21, m	32.2	2.30, d (13.0)	27.4	2.27, dd (13.3, 4.8)
		1.20, dd (14.6, 8.7)		1.79, dd (14.6, 6.2)		1.90, dd (13.3, 10.1)		1.26, dd (13.5, 9.2)
22	43.1	2.36, d (8.5)	42.7	2.37, d (8.6)	41.4	2.22, d (9.8, 4.7)	49.2	2.42, d (9.0)
23	81.2		80.8		83.6		83.0	
24	27.4	0.95, s	26.9	0.97, s	26.3	1.24, s	29.3	1.20, s
25	30.5	1.22, s	29.9	1.23, s	29.2	1.26, s	31.1	1.66, s
OH-1		12.19, s				12.83, s		
OMe-1			55.7	3.84, s			56.0	3.91, s
OMe-3			55.7	3.83, s			55.5	3.80, s
$O\underline{CH_2}CH_3$-8			62.6	3.41, q (7.0)				
$OCH_2\underline{CH_3}$-8			15.0	1.05, t (7.0)				

[a] Assignments are based on DEPT, HSQC, and HMBC experiments. Chemical shifts are given in ppm, *J* in Hz.
[b] Measured in DMSO-d_6.
[c] Measured in $CDCCl_3$. The data in parentheses are coupling constants (*J*) in Hz.

2.4.3. *Garcineobractatin A* (**3**)

Yellow amorphous powder; $[\alpha]_D^{20}$ + 3.0 (*c* 0.10, MeCN); UV (MeOH) λ_{max} (log ε) 204 (3.87), 273 (3.05) and 338 (3.36) nm; IR ν_{max} 2971, 2918, 1746, 1630, 1593, 1448, 1410, 1383, 1317, 1266, 1192, 1082, 1023, 1000, 823, 730, 610, 552, 504, 450 cm^{-1}; ^{1}H NMR (DMSO-d_6, 600 MHz) data, see Table 1; ^{13}C NMR (DMSO-d_6, 150 MHz) data, see Table 2; HRESIMS *m/z* 465.2260 $[M+H]^+$(calced for $C_{28}H_{33}O_6$, *m/z* 465.2277).

(−)-*Garcineobractatin A* (**3a**): t_R 7.4 min; ECD λ_{max} nm (mdeg): 232

Table 2
Cytotoxicity of isolated compounds against cancer cell lines.[a,b]

Compounds	HeLa	A549	PC-3	HT-29	WPMY-1[d]
4	2.57 ± 0.46	1.96 ± 0.30	2.93 ± 0.37	1.11 ± 0.26	0.76 ± 0.11
5	8.10 ± 0.12	9.35 ± 0.55	> 10	> 10	> 10
(−)-**6**	> 10	8.93 ± 0.54	> 10	8.49 ± 1.19	> 10
7	7.10 ± 0.52	6.38 ± 0.73	4.84 ± 1.50	3.10 ± 0.91	3.07 ± 0.60
8	5.30 ± 1.28	4.97 ± 0.96	4.24 ± 0.69	3.46 ± 0.29	2.73 ± 0.34
9	> 10	9.41 ± 0.03	> 10	7.92 ± 1.68	6.23 ± 0.93
10	6.69 ± 0.81	4.12 ± 1.28	3.39 ± 0.48	3.22 ± 0.83	2.54 ± 0.03
11	6.77 ± 0.26	5.28 ± 1.07	8.34 ± 0.71	4.25 ± 1.28	4.96 ± 1.44
12	5.25 ± 1.34	4.68 ± 1.21	7.85 ± 0.89	3.91 ± 1.31	2.65 ± 0.13
13	2.29 ± 0.34	2.22 ± 0.20	4.34 ± 1.73	1.80 ± 0.28	1.17 ± 0.27
14	2.78 ± 0.21	5.19 ± 0.84	2.75 ± 0.07	2.02 ± 0.29	2.23 ± 0.35
15	6.56 ± 0.58	6.00 ± 1.29	2.88 ± 0.09	3.79 ± 1.54	2.05 ± 0.54
16	6.23 ± 0.43	6.13 ± 0.66	4.45 ± 1.19	3.36 ± 0.90	1.76 ± 0.10
Etoposide[c]	12.55 ± 6.01	12.67 ± 1.66	10.07 ± 0.87	16.08 ± 1.72	2.98 ± 0.87

[a] Results are expressed as mean IC_{50} values in μM, and the compounds **1–3** are inactive against these human cancer cell lines (IC_{50} > 10 μM).
[b] Values represent the mean ± SD of three independent experiments.
[c] Positive control.
[d] Human prostatic stromal myofibroblast cell line.

(+7.68), 316 (−3.25) nm.
(+)-*Garcineobractatin A* (***3b***): t_R 15.6 min; ECD λ_{max} nm (mdeg): 228 (−3.82), 310 (+2.48) nm.

2.4.4. Garcibractatin A (4)

Yellow amorphous powder; $[\alpha]_D^{20}$ -12.0 (*c* 0.10, MeCN); UV (MeOH) λ_{max} (log ε) 216 (4.28), 271 (3.45), 322 (3.87), 331 (3.85) and 339 (3.86) nm; IR ν_{max} 2968, 2933, 2850, 1732, 1661, 1617, 1585, 1555, 1469, 1379, 1275, 1213, 1118, 896, 821, 545, 421 cm^{-1}; ^1H NMR ($CDCl_3$, 600 MHz) data, see Table 1; ^{13}C NMR ($CDCl_3$, 150 MHz) data, see Table 2; HRESIMS *m/z* 493.2588 $[M+H]^+$ (calcd for $C_{30}H_{37}O_6$, 493.2590).

(−)-*Garcibractatin A*(***4a***): t_R 9.9 min, 3.6 mg, $[\alpha]_D^{26}$ − 122.3 (*c* 0.036, MeOH); ECD (MeOH) λ_{max} nm ($\Delta\varepsilon$): 205 (+3.92 × 10^3), 235 (+3.63 × 10^2), 302 (+2.42 × 10^3), 344 (−5.13 × 10^3) nm.
(+)-*Garcibractatin A*(***4b***): t_R 11.1 min, 4.4 mg, $[\alpha]_D^{26}$ + 129.5 (*c* 0.044, MeOH); ECD (MeOH) λ_{max} nm ($\Delta\varepsilon$): 205 (−3.56 × 10^3), 234 (−3.43 × 10^3), 301 (−2.55 × 10^3), 343 (+5.51 × 10^3) nm.

2.5. X-ray crystallographic analysis of compounds 1 and 5

Single crystal X-ray diffraction data were collected on a Bruker APEX DUO diffractometer with cross-coupled multilayer optics Cu Kα or Mo Kα radiation. Data were corrected for absorption effects using the multiscan technique (SADABS). The structure was solved by direct methods.

2.5.1. Single-crystal X-ray data for 1

$C_{29}H_{38}O_8$ (*M* = 514.59 g/mol), monoclinic, space group $P2_1/n$ (no. 14), *a* = 11.38510 (10) Å, *b* = 12.87590(10) Å, *c* = 18.3037(2) Å, *β* = 105.58°, *V* = 2584.55(4) $Å^3$, *Z* = 4, *T* = 130 K, μ (CuK$^\alpha$) = 0.784 mm^{-1}, *Dcalc* = 1.322 g/cm^3, 18,969 reflections measured (8.272° ≤ 2Θ ≤ 139.394°), 4813 unique (R_{int} = 0.0250, R_{sigma} = 0.0209) which were used in all calculations. The final R_1 was 0.0382 (I > 2σ(I)) and wR_2 was 0.1044 (all data).

2.5.2. Single-crystal X-ray data for 5

$C_{29}H_{36}O_7$ (*M* = 496.58 g/mol). monoclinic, space group $P2_1/c$ (no. 14), *a* = 14.268(3) Å, *b* = 8.0521(16) Å, *c* = 22.769(4) Å, *β* = 101.986(5)°, *V* = 2558.8 (9) $Å^3$, *Z* = 4, *T* = 205 K, μ(MoKα) = 0.091 mm^{-1}, *Dcalc* = 1.289 g/cm^3, 18,638 reflections measured (2.918° ≤ 2Θ ≤ 55.052°), 5859 unique (R_{int} = 0.0812, R_{sigma} = 0.1009) which were used in all calculations. The final R_1 was 0.0666 (I > 2σ (I)) and wR_2 was 0.2014 (all data). Crystallographic data for compounds **1** and **5** have been deposited at the Cambridge Crystallographic Data Centre with the deposition number CCDC1810860 (for compound **1**) and CCDC1810861(for compound **5**). These data can be obtained free of charge from the Cambridge Crystallographic Data Centre via www.ccdc.cam.ac.uk/data_request/cif.

2.6. Cell viability assay

The cytotoxic activities of all isolates were evaluated by CCK-8 assay using HeLa (human cervical adenocarcinoma), A549 (human lung adenocarcinoma), PC-3 (human prostate cancer), HT-29 (human colorectal adenocarcinoma) and WPMY-1 (normal human prostatic stromal myofibroblast) cell lines. All cell lines from the cell bank of the American Type Culture Collection (ATCC) and the cell bank of the Shanghai Institutes of Biochemistry and Cell Biology, Chinese Academy of Sciences, were maintained at 37 °C with a 5% CO_2 humidified atmosphere in growth medium as recommended by the providers. The positive control compound etoposide (S1225, purity ≥ 98%) was bought from Selleck. The positive control compound and test samples were dissolved in dimethyl sulfoxide (DMSO) to make stock solutions and further diluted in culture medium for assays. The control cells (without treatment) received the same amount of DMSO and were incubated under the same conditions.

Cell proliferation assays were performed as previously described [10,14]: Exponentially growing determined cells were seeded into 96-wells plate at 3 × 10^4 cells per well. After 24 h of incubation, the culture medium was removed and replaced with fresh medium containing the candidate compound at gradient concentrations. The cells were treated for another 72 h. Then, the medium was discarded and replaced with 10% CCK-8 (Dojindo) in complete medium, and the plates were incubated for another 2 h. The absorbance at 450 nm was measured using a micro-plate reader. A background absorbance of the OD_{blank} was subtracted from all wells. The inhibition rate (IR) was determined with the following formula:

$$IR(\%) = (OD_{DMSO} - OD_{compound})/OD_{DMSO} \times 100\%.$$

Each concentration was analyzed in triplicate and the experiment was repeated three times. The average 50% inhibitory concentration (IC_{50}) was determined from the concentration response curves according to the inhibition ratio for each concentration.

3. Results and discussion

3.1. Structure elucidation

The petroleum ether-soluble fraction or upper phase (*n*-hexane-ethyl acetate-95% ethanol-water, 1:1:1:1, v/v/v/v)-soluble fraction of 95% (v/v) EtOH extract of *G. bracteata* was further purified by column chromatography over MCI gel, silica gel, reversed-phase C_{18} silica gel, Sephadex LH-20, and preparative HPLC, yielding sixteen compounds, including four pairs of new (**1**–**4**) and twelve known caged xanthones (Fig. 1 and Fig. S1, Supplementary Material I).

Garcibractone A (**1**) was obtained as a white amorphous powder. Its molecular formula was determined to be $C_{28}H_{34}O_7$ by HRESIMS (*m/z* 483.2387 $[M+H]^+$, calcd. 483.2383). The UV spectrum of **1** showed absorption bands at 217 and 297 nm that were indicative of a caged xanthone derivative lacking a $\Delta^{8(8a)}$ double bond [22–24]. Its IR spectrum indicated the presence of the hydroxy (3406 cm^{-1}) functionality along with unconjugated (1737 cm^{-1}) and conjugated (1639 cm^{-1}) ketone carbonyls. The ^1H and ^{13}C NMR spectroscopic data of compound **1** (Table 1 and Figs. S6–S7, Supplementary Material II) were similar to those of doitunggarcinone L (**5**), isolated from the leaves of *G. propinqua* [24] and *G. bracteata* [22]. The only difference between the structures of compound **1** and doitunggarcinone L was that compound **1** had a C-8 hydroxy group while the latter compound had a C-8 methoxy group, which was consistent with the molecular formula of $C_{28}H_{34}O_7$ deduced by HRESIMS data of compound **1**. The substitution pattern and the assigned structure of **1** were also confirmed by a complete 2D NMR spectra analysis, and selected key correlations in the observed NMR spectra were shown in Fig. 2a and b. The unambiguous assignment of the planar structure and relative configuration of **1** was further confirmed by analysis of the single-crystal X-ray diffraction data (Fig. 3).

The natural caged xanthones were usually found as scalemic mixtures with high enantiomeric ratios of up to 1:2 [22–24]. Although compound **1** showed a specific rotation, $[\alpha]_D^{20}$ − 20.83 (c 0.12, MeCN), this compound might be a scalemic mixture. Therefore, the compound **1** was further resolved via chiral HPLC to give two enantiomers, (−)-**1** ($[\alpha]_D^{26}$ - 9.33, *c* 0.018, MeOH) and (+)-**1** ($[\alpha]_D^{26}$ + 9.63, *c* 0.02, MeOH). The absolute configuration of natural products could be elucidated by comparing experimental ECD spectra with the respective calculated curves [10,11,21–22]. There were only two possible structures of (5*R*, 7*S*, 8*S*, 8a*R*, 10-a*S*, 22*S*)-**1a** and (5*S*,7*R*,8*R*, 8a*S*, 10a*R*, 22*R*)-**1b** for compound **1** by X-ray crystallographic analysis, and the experimental ECD curves of (−)-**1** and (+)-**1** well-matched with the calculated curves of **1a** and **1b** (Fig. 2C). Therefore, the absolute configurations of (−)-**1** and (+)-**1** were determined as **1a** and **1b**, respectively. Moreover, the measurement and

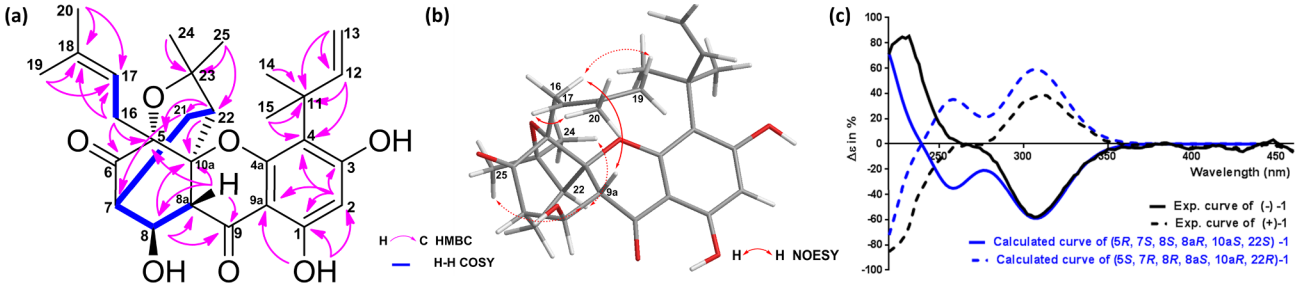

Fig. 2. Key correlations observed in the NMR spectra of (−)-**1**, the experimental curves of (−)-**1** and (+)-**1** and calculated ECD spectra of **1a** and **1b**.

calculation of specific rotations was often used to assign the absolute configuration of natural products [25,26]. A pair of the two enantiomers had usually equal but opposite specific rotations, and hence the absolute configurations of two enantiomers could be assigned by comparison of experimental specific optical rotations (OR, $[\alpha]_D$ values) with the respective calculated OR values. Compound **1** was a pair of two enantiomers which was confirmed by X-ray crystallographic and HPLC-ECD analysis (Fig. 4a, Fig. S13, Supplementary Material II), and the OR values of (5*R*, 7*S*, 8*S*, 8a*R*, 10-a*S*, 22*S*)-**1a** and (5*S*,7*R*,8*R*, 8a*S*, 10a*R*, 22*R*)-**1b** were calculated at B3LYP/6-311 + + G (d, p) //B3LYP/6-31G (d, p) level with a PCM model in MeOH solvent. The experimental OR values of $[\alpha]_D^{26}$ − 9.33 (*c* = 0.018 in MeOH) for (−)-**1** and $[\alpha]_D^{26}$ + 9.63 (*c* = 0.02 in MeOH) for (+)-**1** had the same algebraic sign as the calculated OR values of $[\alpha]_D$ = −166 for **1a** and $[\alpha]_D$ = +163 for **1b** (Table CS2, Supplementary Material I), and hence the absolute configurations of (−)-**1** and (+)-**1** could be assigned as **1a** and **1b**, respectively. The assignments of absolute configurations of (−)-**1** and (+)-**1** were also consistent with that by measurement and calculation of ECD spectra. Thus, the structures of (−)-**1** and (+)-**1** were unambiguously determined as shown.

Garcibractone B (**2**) showed an ion peak at *m/z* 539.3010 $[M+H]^+$, yielding the molecular formula $C_{32}H_{42}O_7$. The UV spectra of this compound resembled those of **1**. The NMR data for **2** were similar to the NMR data of **1**, indicating that the two compounds have similar carbon skeletons; however, The NMR data indicated that two methoxy groups [δ_H 3.84 (3H, s, CH_3O-1), 3.83 (3H, s, CH_3O-3); δ_C 55.7 (CH_3O-1), and 55.7 (CH_3O-3)] and an ethyoxy group [δ_H 3.44 (2H, m, $CH_3\underline{CH_2}O$–), 1.06 (3H, t, *J* = 7.0 Hz, $\underline{CH_3}CH_2O$–); δ_C 62.7 ($CH_3\underline{CH_2}O$–), and 14.9 ($\underline{CH_3}CH_2O$–)] were present in **2** instead of three hydroxyl groups in **1**. The HMBC correlations observed from H at δ_H 3.84 to C-1 (δ_C 160.5), H at δ_H 3.83 to C-3 (δ_C 165.1) and H at δ_H 3.44 to C-8 (δ_C 72.7) and $\underline{CH_3}CH_2O$– (δ_C 14.9) confirmed the locations of methoxy and ethyoxy groups in **2**. The 2D structure of **2** was further confirmed by a detailed NMR analysis, and the selected key correlations observed in the H−H COSY and HMBC spectra were shown in Fig. 5a. The complete assignments of the ^1H and ^{13}C spectroscopic data of **2** were summarized in Table 1.

The relative configuration of **2** was also determined to be identical to that of **1** based on the NOESY data and the similar ^1H and ^{13}C chemical shifts of the caged scaffold at the C ring of the xanthone moiety, the selected key correlations observed in the NOESY were shown in Fig. 5b. The α_D value of **2** was very low ($[\alpha]_D^{24}$ = 0.91, *c* 0.101, MeCN), implying that compound **2** might be also a scalemic mixture. Chiral HPLC-ECD analysis showed two peaks in a ratio of ca. 1.1:1 (Fig. S28, Supplementary material II). Compound **2** was further separated by semi-preparative chiral HPLC to afford (+)-**2** ($[\alpha]_D^{25}$ + 24.44, *c* 0.09, MeCN) and (−)-**2** ($[\alpha]_D^{25}$ –23.33, *c* 0.09, MeCN). By the comparisons of their HPLC-ECD spectra of (+)-**2** and (−)-**2** with those of (+)-**1** and (−)-**1**, (−)-**5** and (+)-**5**, and (−)-**6** and (+)-**6**, the measured ECD spectra of (+)-**2** and (−)-**2**, (−)-**5** and (+)-**5**, and (−)-**6** and (+)-**6** showed the same cotton effects as that of compounds (+)-**1** and (−)-**1**, which revealed that these compounds had the same absolute configuration (Fig. 4b). Therefore, the absolute configurations of (−)-**2** and (+)-**2** could be determined as (5*R*, 7*S*, 8*S*, 8a*R*, 10-a*S*, 22*S*)-**2a** and (5*S*, 7*R*, 8*R*, 8a*S*, 10a*R*, 22*R*)-**2b**, respectively. In addition, the OR values of **2a** and **2b** were calculated at B3LYP/6-311 + + G (d, p) //B3LYP/6-31G (d, p) level with a PCM model in MeOH solvent. The experimental OR values of $[\alpha]_D^{25}$ –23.33 (*c* = 0.09 in MeCN) for (−)-**2** and $[\alpha]_D^{25}$ + 24.44 (*c* = 0.09 in MeCN) for (+)-**2** had the same algebraic sign as the calculated OR values of $[\alpha]_D$ = −154 for **2a** and $[\alpha]_D$ = +36 for **2b** (Table CS4, Supplementary Material I), and hence the absolute configurations of (−)-**2** and (+)-**2** could also be assigned as **2a** and **2b**.

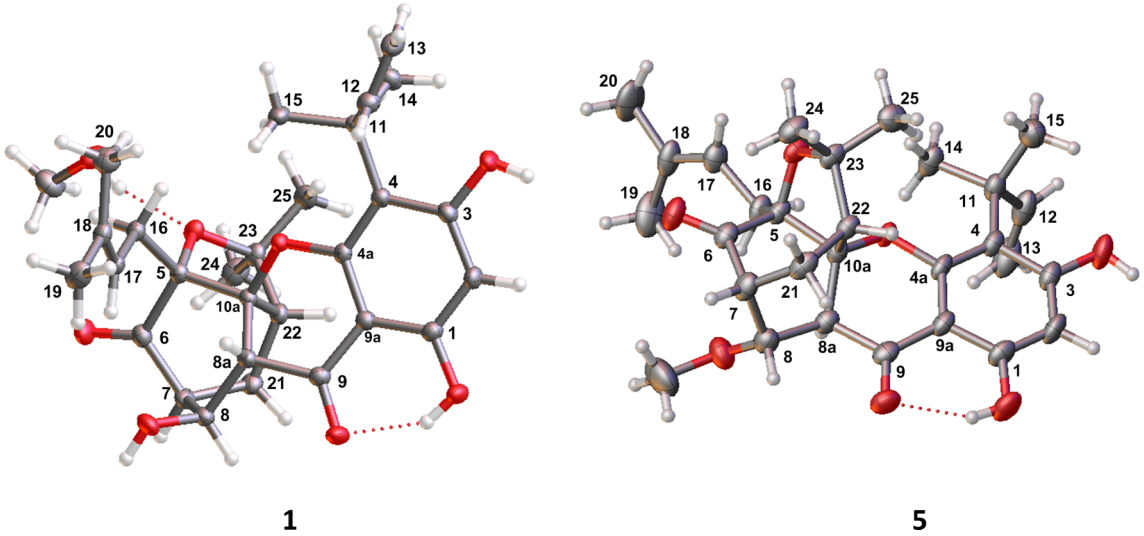

Fig. 3. X-ray ORTEP diagram of **1** and **5**.

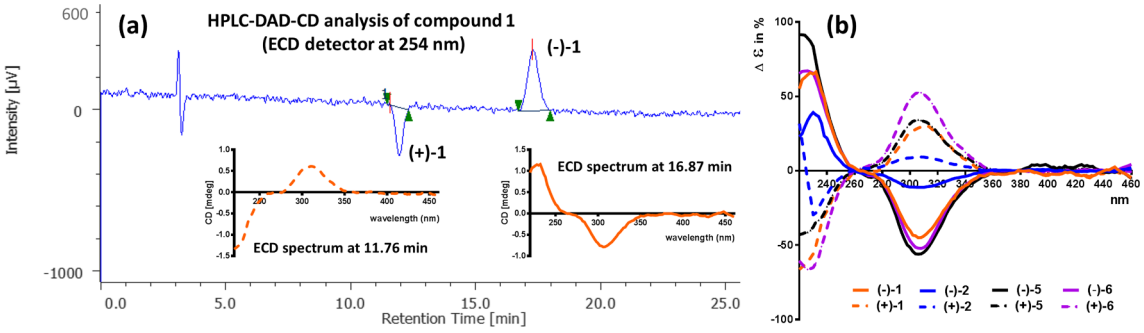

Fig. 4. (a) Resolution of **1** on the chiral AD-H column monitored at 254 nm. (b) The experimental ECD spectra of (−)-**1**, (+)-**1**, (−)-**2**, (+)-**2**, (−)-**5**, (+)-**5** and (−)-**6**, and (+)-**6.**

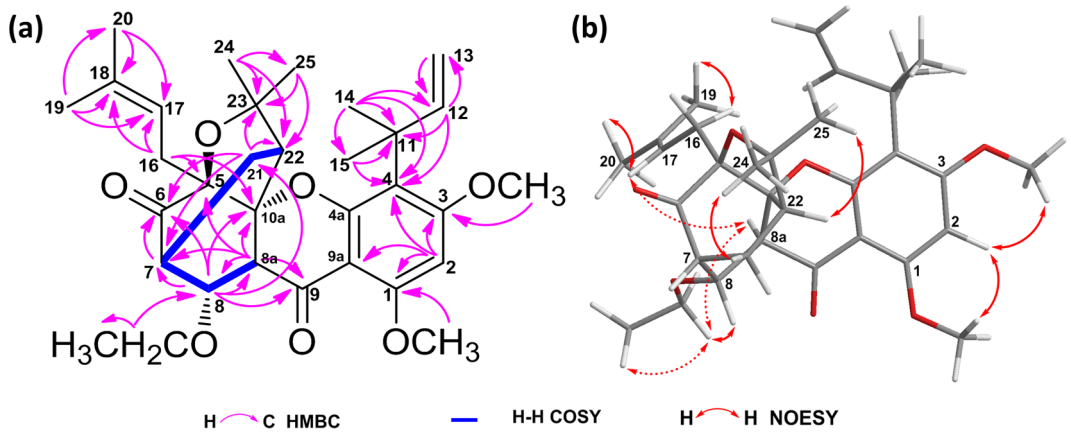

Fig. 5. Key correlations observed in the NMR spectra for (+)-**2.**

Consequently, the structures of (+)-**2** and (−)-**2** were established as shown.

Garcineobractatin A (**3**) was isolated as a yellow amorphous powder with a molecular formula of $C_{28}H_{32}O_6$ as determined by HRESIMS (*m/z* 465.2260 $[M+H]^+$, calcd for 465.2277). The ^1H and ^{13}C NMR data (Table 1) were also comparable to the neocaged xanthone, including the presence of ^{13}C NMR resonances typical of unconjugated and conjugated ketone carbonyls at δ_C 200.1 (C-5) and 178.9 (C-9) [16–18,22,27–28]. Except for the substituent at C-2 and C-4, the NMR data of **3** were similar to those of neobractatin [16]. The NMR data indicated a prenyl group [δ_H 3.09 (2H, dd, J = 7.3 Hz, H-11), 5.11 (1H, dd, J = 5.9, 7.3 Hz, H-12), 1.60 (3H, s, H_3 -14), and 1.68 (3H, s, H_3-15); δ_C 20.6 (C-11), 122.7 (C-12), 129.6 (C-13), 25.4 (C-14), and 17.6 (C-15)] at C-2 in **3** instead of a 1,1- dimethylprop-2-en-1-yl group at C-4 in neobractatin. The HMBC correlations observed from H_2-11 to C-1 (δ_C 161.1) and C-2 (δ_C 108.4), together with the molecular formula of $C_{28}H_{32}O_6$, confirmed the above deduction. The 2D structure of **3** was further confirmed by a detailed 2D NMR spectra analysis, and the selected key correlation observed in H−H COSY and HMBC spectra were shown in Fig. 6a.

The relative configuration of **3** was assessed by analysis of the NOESY data. NOESY correlations were observed between H-8 and H-7, H-7 and H-25, H-25 and H-22, H-22 and H-21b, and H-24 and H-21a (Fig. 6b), which supported the same relative stereochemistry for the tricyclic core of **3** as previously reported for the caged xanthones [22,27,28]. Due to the α_D value ($[\alpha]_D^{25}$ = 3.0, *c* 0.1, MeCN), **3** was further analyzed by online chiral HPLC-ECD which showed well-resolved peaks for two enantiomers in a ratio of ca. 1:1.1 (Fig. 6c and Fig. S43, Supplementary Material II). The absolute configurations of **3a** and **3b** were assigned as (6*S*, 7*R*, 10a *S*, 22*S*) and (6*R*, 7*S*, 10a *R*, 22*R*) by comparing the experimental and calculated ECD spectra (Fig. 6d). Although the pure enantiomers of compound **3** could not be obtained due to the small amount of compound remaining, compound **3** was a pair of two enantiomers which had be confirmed by the HPLC-ECD analysis (Fig. 6c). The OR values of two candidate structures of (6*S*, 7*R*, 10a *S*, 22*S*)-**3a** and (6*R*, 7*S*, 10a *R*, 22*R*)-**3b** were calculated to give values of $[\alpha]_D$ = −46 for **3a** and $[\alpha]_D$ = +44 for **3b** (Table CS6, Supplementary Material I), respectively. The results showed that **3a** was the levorotatory or (−)-isomer and **3b** was the dextrorotary or (+)-isomer of compound **3**. Therefore, the absolute configurations of (−)-**3** and (+)-**3** could be identified as **3a** and **3b** based on the experimental and calculated ECD spectra and calculation of specific rotations, and the structures of (−)-**3** and (+)-**3** were established as shown.

Garcibractatin A (**4**) was obtained as a yellow amorphous powder. A molecular formula of $C_{30}H_{36}O_6$ was suggested by HRESIMS (*m/z* 493.2588 $[M+H]^+$, calcd for 493.2590). The UV absorption maxima at 215 and 341 nm were indicative of a caged xanthone derivative with a $\Delta^{8(8a)}$ double bond [11,16,22]. The NMR data of **4** were similar to those of bractatin (**8**) isolated from the same plant [16], indicating that the two compounds had similar carbon skeletons. The NMR data indicated that two methoxy groups [δ_H 3.91 (3H, s, C$\underline{H}_3$O-1)/δ_C 56.0 (C$\underline{H}_3$O-1) and 3.80 (3H, s, C$\underline{H}_3$O-3)/δ_C 55.5 (C$\underline{H}_3$O-3)] were present in **4** replaced by two hydroxyl groups in bractatin (**8**) [16]. The HMBC correlations observed from H at δ_H 3.91 to C-1 (δ_C 161.1) and H at δ_H 3.80 to C-3 (δ_C 165.5), together with the molecular formula of $C_{30}H_{36}O_6$, confirmed the locations of two methoxy groups. The 2D structure of **5** was further confirmed by a detailed H−H COSY and HMBC analysis (Fig. 7a), and the complete assignments of the ^1H and ^{13}C spectroscopic data of **4** are summarized in Table 1.

The relative configuration of **4** was assessed by analysis of the NOESY data. NOESY correlations were observed between H-24 and H-21b, H-25 and 22, H-22 and H-21b (Fig. 7b), which supported the same relative stereochemistry for the tricyclic core of **4** as previously reported for caged xanthonoids [11,16–18,22–24]. Compound **4** was

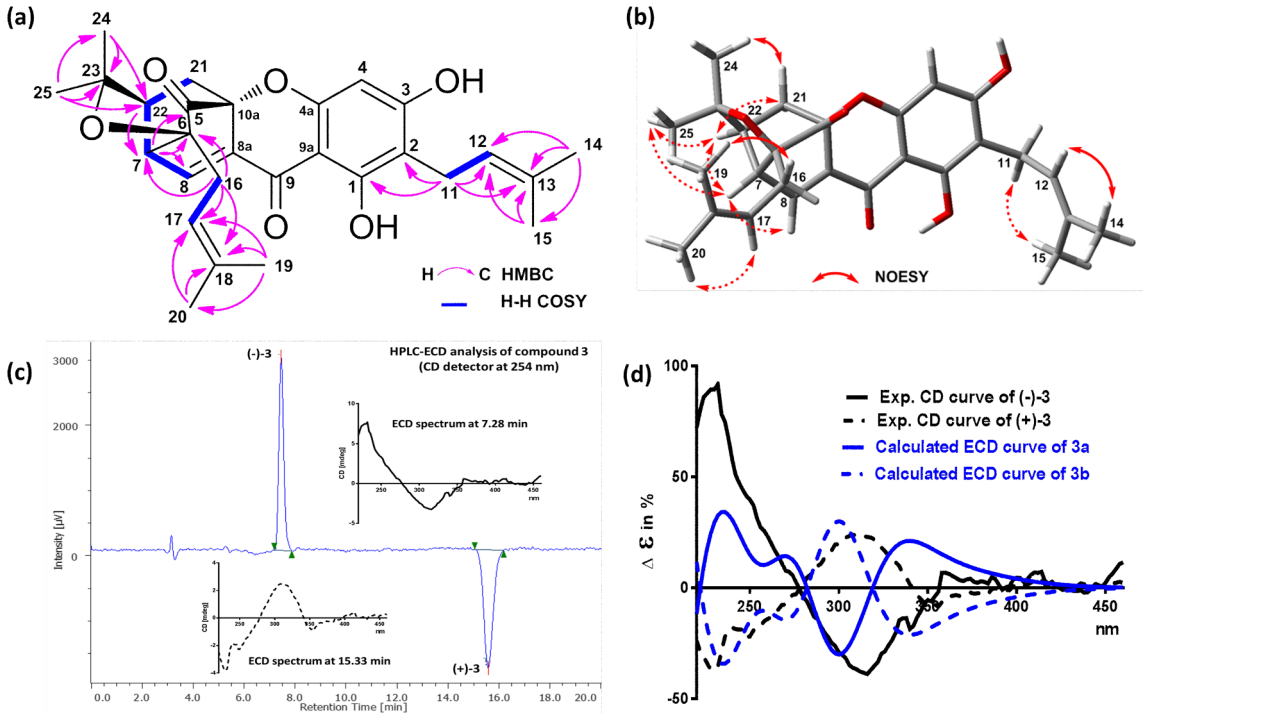

Fig. 6. (a) Selected key correlations observed in the HMBC and H−H COSY spectra of (−)-**3**. (b) Selected key correlations observed in the NOESY spectra of (−)-**3**. (c) Resolution of compound **3** on the chiral AD-H column monitored at 254 nm. (d) the experimental curves of (−)-**3** and (+)-**3** and TD-DFT calculated ECD spectra of **3a** and **3b**.

resolved by chiral HPLC on an AD-H column to yield the two enantiomers (−)-**4** ($[\alpha]_D^{26}$ − 122.3, *c* 0.036, MeOH) and (+)-**4** ($[\alpha]_D^{26}$ + 129.5, *c* 0.044, MeOH). The absolute configurations of (−)-**4** with specific rotation ($[\alpha]_D^{26}$ − 122.3, *c* 0.036, MeOH) could be assigned as (5*R*, 7*S*, 10a *S*, 22*S*)-**4a** by comparison of the experimentally measured ECD curves with the calculated curves (Fig. 7c), and the absolute configurations of (+)-**4** could be defined as (5*S*, 7*R*, 10a *R*, 22*R*)-**4b** from the opposite ECD spectra (Fig. 7c). Moreover, the OR values **4a** and **4b** were calculated, and the experimental OR values of $[\alpha]_D^{26}$ –122.3 (*c* = 0.036 in MeOH) for (−)-**4** and $[\alpha]_D^{26}$ + 129.5 (*c* = 0.044 in MeOH) for (+)-**4** had the same algebraic sign as the calculated OR values of $[\alpha]_D$ = −653 for **4a** and $[\alpha]_D$ = +559 for **4b** (Table CS8, Supplementary Material I). As a result, the absolute configurations of (−)-**4** and (+)-**4** were determined by the experimental and calculated ECD spectra and specific rotations, and the structures of (−)-**4** and (+)-**4** were established unambiguously as shown.

The structures of doitunggarcinone L (**5**) [22,23], 8-ethoxy-8,8a-dihydrobractatin (**6**) [22], cochinchinoxanthone (**7**) [29], bractatin (**8**) [16,29], 1-*O*-methylbractatin (**9**) [16], isobractatin (**10**) [16], 1-*O*-methylisobractatin (**11**) [16], epiisobractatin (**12**) [22,30], forbesione (**13**) [31], isoforbesione (**14**) [31], neobractatin (**15**) [18], and 3-*O*-methyl-neobractatin (**16**) [18] were elucidated by comparing the physicochemical and spectroscopic data with the reported values. The planar structure and relative configuration of **5** was further confirmed by X-ray diffraction analysis (Fig. 3). Of these isolates, garcibractones A-B (**1–2**) and compound **5–6** were the rare 8,8a-dihydro caged xanthones that had been isolated and identified only from several species of the Garcinia genus until now [32–33], including *G. hunburyi* [34–35], *G. morella*, *G. gaudichaudii* [36], *G. scortechinii* [37], *G. bracteata* [16,18], *G. lateriflora* [38], and *G. propinqua* [23–24]. Garcineobractatin A (**3**) and compound **15–16** were an unusual neocaged xanthone type with the ketone group at C-5 typified by neobractatin [16,22], which have only been isolated from *G. bracteata* [16–18,21,22], *G. edulis* [27] and *Cratoxylum formosum* ssp. Pruniflorum [28] until now.

Most of the isolated compounds were analyzed by the chiral HPLC-ECD, and all of compounds **1–7**, **9**, **12–16** were found as scalemic mixtures (Fig. S6, Supplementary Material I). Compounds **1**, **2**, **5** and **6** showed well-matched ECD spectra (Fig. 4b), compounds **3**, **15** and **16** displayed similar ECD spectra (Fig. S2, Supplementary material I), and compounds **4**, **7**, **9**, **12**, **13** and **14** also exhibited well-matched ECD spectra (Fig. S5, Supplementary material I). Compounds **7**, **9**, and **13–14** were found as scalemic mixtures in nature for the first time. The results also showed that the absolute configurations of enantiomers of

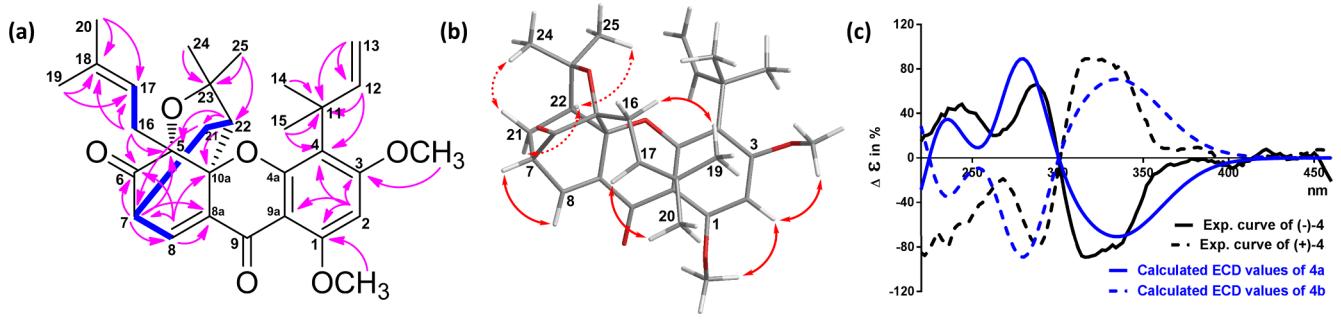

Fig. 7. Key correlations observed in the NMR spectra of (−)-**4**, the experimental curves of (−)-**4** and (+)-**4** and TD-DFT calculated ECD spectra of **4a** and **4b**.

new compounds **1**, **3** and **4** could be determined by online measurement and theoretical calculation of ECD spectra and specific rotations. Our findings indicated that an effective method for the resolution of racemic mixture could be established by combination of chiral HPLC-ECD analysis and the calculations of ECD spectra and specific rotations, and HPLC-ECD analysis has been proven to be a fast, reliable, and chemical-saving analytical approach for scalemic mixtures from natural sources.

It was noteworthy that compounds **2**, **5**, and **6** with 8-*O*-methyl or 8-*O*-ethoxy groups were usually believed to be MeOH- or EtOH-addition products of enone precursor (such as compound **8**). To determine whether these compounds were naturally occurring, a simple and rapid LC-HRMS method had been developed for determination of the chemical composition of the $CHCl_3$ extract of *G. bracteata* leaves. LC-HRMS analysis showed that compounds **5–6** could be found from the $CHCl_3$ extract of *G. bracteata* leaves (Figs. S7–S8, Supplementary material I), and hence the 8-*O*-methyl or 8-*O*-ethoxy products should be not artifacts. The results were consistent with reported results [22].

3.2. Anti-proliferative activity

All isolates were evaluated for their cytotoxic activity against human HeLa, A549, PC3, HT-29, and WPMY-1 cells. As shown in Table 2, compounds **4–16** exhibited significant cytotoxic activity against two or four human cancer cell lines with IC_{50} values ranging from 1.11 to 9.41 μM, which are better than the positive control etoposide in most cases. In the cases of A549 and HT-29 cells, garcibractatin A (**4**) was found to be more active than the other compounds with IC_{50} values of 1.11 and 1.96 μM, compound **13** showed the most potent cytotoxicity against HeLa cells with an IC_{50} value of 2.29 μM, and compound **14** displayed the highest activity against PC-3 cells with an IC_{50} value of 2.75 μM.

Of these compounds, the caged xanthones (**4**, **7–14**) seemed to be more active than the neocaged xanthones (**3**, **15–16**), and the neocaged xanthones seemed to be more active than the 8,8a-dihydro caged xanthones (**1–2, 5** and **6**). For instance, the caged xanthones **4** and **14** were the most effective compounds against HeLa, PC-3 and HT-29 cells with IC_{50} values ranging from 1.11 to 2.93 μM, while **4** and **13** were the most effective compounds against HeLa, A549 and HT-29 cells with low micro-molar IC_{50} values (1.11–2.57 μM). Similarly, compounds **15–16** were found to be more active than **1–3**, **5** and **6**. This finding showed that the double bond at C-8/C-8a of the caged xanthone might be a crucial structural element for cytotoxicity which was in accordance with previous findings [22–24,30,31].

The inhibitory activities of compounds **13** and **14**, which possess prenyl groups in the non-caged region (A ring) of the caged xanthone, were more potent than the inhibitory activities of the corresponding caged xanthone compound **7**. The different prenyl substitution in the non-caged region of the caged xanthone showed a significant influence on the activity against the different human cancer cells. Compound **13**, for example, bearing a prenyl group at C-4, was found to be more active against HeLa, A549, and HT-29, and about 1-fold more active against A549 cells than compound **14** with a prenyl group at C-2. Meanwhile, compound **13** showed the about 1-fold less activity than compound **14** in the case of PC-3 cells. The prenyl group in the non-caged region of the caged xanthone also showed more activity against the different human cancer cells than the 1,1-dimethylallyl group. Compared with compound **8**, compound **13** showed approximately 1-fold more activity against HeLa, A549, and HT-29 cells. At the same time, the cyclization of the group into a furan ring (such as **10**) did not significantly influence the activity of the corresponding compound **8**. These data indicated that the prenyl group in the non-caged region of the caged xanthone might be crucial for antitumor activity, which were consistent with the reported results [22].

Compounds (**9**, **11**, and **16**) with methoxy group at C-1 or C-3 showed approximately 1-fold less activity against PC-3 cells than the corresponding compounds (**8, 10**, and **15**) with hydroxyl group, and hence methylation of the hydroxyl group at C-1 showed more significant influence on the activity against human cancer cells than methylation of the hydroxyl group at C-3. This finding is consistent with the reported results [23,29,30]. However, compounds (**2** and **4**) with bi-methoxy group at C-1 and C-3 showed more activity against the human cancer cells than the corresponding compounds (**6** and **8**) with hydroxyl group. It was interesting that bi-methylation of the hydroxyl group (such as **2** and **4**) at C-1 and C-3 was found to show a more significant positive influence on the cytotoxicity than methylation of the hydroxyl group at C-1 or C-3.

Notably, only (−)-**6 (**the levorotatory enantiomer of compound **6**) had cytotoxicity while (+)-6 (its counterpart enantiomer) or compound **6** (racemic mixture) was inactive. In addition, only compounds (−)-**6** and **5** in Table 2 did not show cytotoxicity toward the normal human prostatic stromal myofibroblast cell line (WPMY-1) among these cytotoxic compounds, indicating some selective toxicity toward cancer cells. These results showed that the two enantiomers from scalemic mixture might show considerably different cytotoxicity and lead to some selective toxicity toward cancer cells.

4. Conclusions

In the paper, four pairs of previously undescribed caged xanthones (**1–4**) and twelve known caged xanthones (**5–16**) were isolated from an extract of the leaves of *G. bracteata*. Of these isolates, garcibractones A-B (**1–2**) and compound **5–6** were the rare 8,8a-dihydro caged xanthones, while garcineobractatin A (**3**) and compound **15–16** were an unusual neocaged xanthone type. The absolute configurations of new caged xanthones **1**, **3**, and **4** could be determined by the combination of two different chiroptical methods including measurement and calculation of electronic circular dichroism (ECD) spectra and specific rotations. The online HPLC-ECD approach was applied to allow a fast, reliable, and chemical-saving analysis, which can be confirmed to be suitable for the analysis of scalemic mixtures.

Although the synthesized caged xanthones based on gambogic acid were designed to gain an understanding of the structure-activity relationship around the pharmacophoric caged core for antitumor activity [39,40], the structure-activity relationship of the natural caged xanthones has not been fully discussed. The structure-activity relationship of the natural caged xanthones with three different caged cores was discussed from the cytotoxic data of isolates in the paper for the first time, and the effects of the substitution of variant groups were also discussed at the same time. Some helpful preliminary conclusions have been drawn: (a) The cytotoxic activities of 8,8a-dihydro-caged xanthones were less potent than that of the corresponding neocaged xanthones, and the neocaged xanthones were less active than the corresponding caged xanthones; (b) The prenyl group in the non-caged region of a caged xanthone might be crucial for antitumor activity; (c) Bi-methylation of the hydroxyl group (such as **2** and **4**) at C-1 and C-3 was found to show a more significantly positive influence on the cytotoxicity; (d) The enantiomer and its counterpart enantiomer of some 8,8a-dihydro-caged xanthones might show different cytotoxicity, and some selective toxicity toward cancer cells.

Acknowledgments

We are grateful for the financial support from the Natural Science Foundation of China (Nos. 81602990), Professor of Special Appointment (Eastern Scholar) at Shanghai Institutions of Higher Learning and the Foundation of Shanghai University of Traditional Chinese Medicine (2016YSN06).

Appendix A. Supplementary material

Supplementary data to this article can be found online at https://doi.org/10.1016/j.bioorg.2018.10.041.

References

[1] D.J. Newman, J. Med. Chem. 51 (2008) 2589–2599.
[2] G.M. Cragg, D.J. Newman, Biochim. Biophys. Acta 1830 (2013) 3670–3695.
[3] H. Yao, J.K. Liu, S.T. Xu, Z.Y. Zhu, J.Y. Xu, Expert Opin. Drug Discov. 12 (2017) 121–140.
[4] D.J. Newman, G.M. Cragg, J. Nat. Prod. 79 (2016) 629–661.
[5] G.M. Cragg, D.J. Newman, J. Ethnopharmacol. 100 (2005) 72–79.
[6] A. Rayan, J. Raiyn, M. Falah, PLoS One 12 (2017) e0187925.
[7] W.M. Fu, J.F. Zhang, H. Wang, Z.C. Xi, W.M. Wang, P. Zhuang, X. Zhu, S.C. Chen, T.M. Chan, K.S. Leung, G. Lu, H.X. Xu, H.F. Kung, J. Proteom. 75 (2012) 4833–4843.
[8] C. Feng, S.X. Huang, X.M. Gao, H.X. Xu, Kathy Luo, J. Nat. Prod. 77 (2014) 1111–1116.
[9] Y.Z. Lao, G. Wan, Z.Y. Liu, X.Y. Wang, P. Ruan, W. Xu, D.Q. Xu, W.D. Xie, Y. Zhang, H.X. Xu, N.H. Xu, Autophagy 10 (2014) 1–14.
[10] W.W. Fu, M. Wu, L.L. Zhu, Y.Z. Lao, L.P. Wang, H.S. Tan, Q.H. Yuan, H.X. Xu, RSC Adv. 5 (2015) 78259–78267.
[11] Y.X. Tang, W.W. Fu, R. Wu, H.S. Tan, Z.W. Shen, H.X. Xu, J. Nat. Prod. 79 (2016) 1752–1761.
[12] Z.C. Xi, M. Yao, Y. Li, C.L. Xie, J. Holst, T. Liu, S.F. Cai, Y.Z. Lao, H.S. Tan, H.X. Xu, Q.H. Dong, Cell Death Dis. 7 (2016) e2252.
[13] L. Zhang, J.L. Feng, S.Y. Kong, M. Wu, Z.C. Xia, B.J. Zhang, W.W. Fu, Y.Z. Lao, H.S. Tan, H.X. Xu, Cancer Lett. 380 (2016) 447–456.
[14] D.Q. Xu, Y.Z. Lao, N.H. Xu, H. Hu, W.W. Fu, H.S. Tan, Y.Z. Gu, Z.J. Song, P. Cao, H.X. Xu, Planta Med. 81 (2015) 79–89.
[15] H.W. Li, J. Li, P.F. Stevens, Flora of China, vol. 13, Beijing 2011, pp. 40–47.
[16] O. Thoison, J. Fahy, V. Dumontet, A. Chiaroni, C. Riche, M.V. Tri, T. Sévenet, J. Nat. Prod. 63 (2000) 441–446.
[17] O. Thoison, D.D. Cuong, A. Gramain, A. Chiaroni, N.V. Hung, T. Sevenet, Tetrahedron 61 (2005) 8529–8535.
[18] Z. Na, H.B. Hu, Q.F. Fan, Helv. Chim. Acta 93 (2010) 958–963.
[19] S.L. Niu, Z.L. Li, F. Ji, G.Y. Liu, N. Zhao, X.Q. Liu, Y.K. Jing, H.M. Hua, Phytochemistry 77 (2012) 280–286.
[20] Y.K. Li, Z.Y. Wang, X.X. Wu, Y.C. Yang, Y. Qin, C.F. Xia, Y.L. Meng, M. Li, X.M. Gao, Q.F. Hu, Phytochem. Lett. 11 (2015) 24–27.
[21] S.L. Niu, D.H. Li, Y.T. Wang, K.B. Wang, B. Lin, Y.K. Jing, H.M. Hua, J. Bai, Z.L. Li, Org. Biomol. Chem. 15 (2017) 4901–4906.
[22] S.L. Niu, D.H. Li, X.Y. Li, Y.T. Wang, S.G. Li, J. Bai, Y.H. Pei, Y.K. Jing, Z.L. Li, H.M. Hua, J. Nat. Prod. 81 (2018) 749–757.
[23] T. Sriyatep, R.J. Andersen, B.O. Patrick, S.G. Pyne, C. Muanprasat, S. Seemakhan, S. Borwornpinyo, S. Laphookhieo, J. Nat. Prod. 80 (2017) 1658–1667.
[24] T. Sriyatep, C. Tantapakul, R.J. Andersen, B.O. Patrick, S.G. Pyne, C. Muanprasat, S. Seemakhan, S. Borwornpinyo, S. Laphookhieo, Fitoterapia 124 (2017) 34–41.
[25] P.J. Stephens, J.J. Pan, F.J. Devlin, J.R. Cheeseman, J. Nat. Prod. 71 (2008) 285–288.
[26] J. Podlech, S.C. Fleck, M. Metzler, J. Bürck, A.S. Ulrich, Chem. Eur. J. 20 (2014) 11463–11470.
[27] J.J. Magadula, Fitoterapia 81 (2009) 420–423.
[28] N. Boonnak, S. Chantrapromma, H.K. Fun, S. Yuenyongsawad, B.O. Patrick, W. Maneerat, D.E. Williams, R.J. Andersen, J. Nat. Prod. 77 (2014) 1562–1571.
[29] Y. Ren, S. Matthew, D.D. Lantvit, T.N. Ninh, H. Chai, J.R. Fuchs, D.D. Soejarto, E.J. de Blanco, S.M. Swanson, A.D. Kinghorn, J. Nat. Prod. 74 (2011) 1117–1125.
[30] Sri. Hartati, I. Ketut Triyono, Sri. Handayani, Indonesian J. Chem. 14 (2014) 277–282.
[31] E.J. Tisdale, I. Slobodov, E.A. Theodorakis, PNAS 101 (2004) 12030–12035.
[32] Q.B. Han, H.X. Xu, Curr. Med. Chem. 16 (2009) 3775–3796.
[33] N. Anantachoke, P. Tuchinda, C. Kuhakarn, M. Pohmakotr, V. Reutrakul, Pharm. Biol. 50 (2012) 78–91.
[34] J. Asano, K. Chiba, M. Tada, T. Yoshii, Phytochemistry 41 (1996) 815–820.
[35] S.J. Tao, S.H. Guan, W. Wang, Z.Q. Lu, G.T. Chen, N. Sha, Q.X. Yue, X. Liu, D.A. Guo, J. Nat. Prod. 72 (2009) 117–124.
[36] Y.J. Xu, S.C. Yip, S. Kosela, E. Fitri, M. Hana, S.H. Goh, K.Y. Sim, Org. Lett. 2 (24) (2000) 3945–3948.
[37] V. Rukachaisirikul, P. Painuphong, Y. Sukpondma, S. Koysomboon, P. Sawangchote, W. Taylor, J. Nat. Prod. 66 (2003) 933–938.
[38] Y.L. Ren, D.D. Lantvit, E.J. Carcache de Blanco, L.B.S. Kardono, S. Riswan, H. Chai, C.E. Cottrell, N.R. Farnsworth, S.M. Swanson, Y. Ding, X.C. Li, J.P.J. Marais, D. Ferreira, A.D. Kinghorn, Tetrahedron 66 (2010) 5311–5320.
[39] X.J. Zhang, X. Li, H.P. Sun, X.J. Wang, L. Zhao, Y. Gao, X.R. Liu, S.L. Zhang, Y.Y. Wang, Y.R. Yang, S. Zeng, Q.L. Guo, Q.D. You, J. Med. Chem. 56 (2013) 276–292.
[40] X.L. Xu, Y. Wu, M.Y. Hu, X. Li, C.Y. Gu, Q.D. You, X.J. Zhang, Bioorg. Med. Chem. 24 (2016) 4626–4635.